distortion therefore explains the magnetoelectric coupling. Application of the electric field transfers the sample into a single-domain state with maximum field **D** for which transition into the $P6_3\underline{cm}$ phase leads to the largest possible energy gain from $H_{ME} = \hat{\alpha}\mathbf{DB}$. According to ref. 13 and Fig. 4a up to 40% (Ho^{3+}: 3–4μ_B) of the rare-earth spins are ordered. The increase defining T_{Ho} in Figs 2a and 4 is due to Ho^{3+}–Ho^{3+} exchange in the x–y plane which complements the Ho^{3+}–Mn^{3+} interaction.

Transition into the magnetoelectric $P6_3\underline{cm}$ phase corresponds to modification of the inter-planar Mn^{3+}–Mn^{3+} exchange paths stabilizing the three-dimensional magnetic order. With the Mn^{3+} ions at $x = \frac{1}{3}a$, the inter-planar Mn^{3+}–Mn^{3+} exchange is nearly perfectly frustrated. Frustration is overcome by the ~2% movement of the Mn^{3+} ions revealed in Figs 1 and 4b. Depending on the shift being positive or negative, either the exchange path favouring formation of the $\underline{6}_3$ axis (above T_{Ho} at $E = 0$) or the exchange path favouring formation of the 6_3 axis (below T_{Ho} at $E = 0$ and below T_N at $E = \pm E_0$) is strengthened. Figure 4c shows that the electric dipole moment is modified along with the magnetic transition which is another manifestation of magnetoelectric interaction on the microscopic scale.

Thus we have observed how multifold magnetic ordering in $HoMnO_3$ is controlled by a static electric field. Ferromagnetic Ho^{3+} ordering is deliberately activated or deactivated, and the ferromagnetic component is controlled by the sign of the electric field. The driving mechanism for phase control are microscopic magnetoelectric interactions originating in the interplay of Ho^{3+}–Mn^{3+} interaction and ferroelectric distortion. With their potential for giant magnetoelectric effects, magnetic ferroelectrics are most favourable for technological applications of magnetoelectric switching, which is reflected by the current push for novel compounds and concepts to understand this class of materials[27,28]. On the basis of the work presented here, promising candidates for controlled magnetoelectric switching[10] are compounds with electronic states close to the ground state which are energetically lowered by magnetoelectric contributions in an applied electric or magnetic field. Therefore frustrated systems or systems in the vicinity of phase boundaries or quantum critical points[29] are prime candidates for magnetic phase control by an electric field or vice versa. □

Received 19 April; accepted 8 June 2004; doi:10.1038/nature02728.

1. Prinz, G. A. Magnetoelectronics applications. *J. Magn. Magn. Mater.* **200,** 57–68 (1999).
2. Ohno, H. *et al.* Electric-field control of ferromagnetism. *Nature* **408,** 944–946 (2000).
3. Asamitsu, A., Tomioka, Y., Kuwahara, H. & Tokura, Y. Current switching of resistive states in magnetoresistive manganites. *Nature* **388,** 50–52 (1997).
4. O'Dell, T. H. *The Electrodynamics of Magneto-electric Media*, (North-Holland, Amsterdam, 1970).
5. Schmid, H. On a magnetoelectric classification of materials. *Int. J. Magn.* **4,** 337–361 (1973).
6. Nan, C. W. *et al.* A three-phase magnetoelectric composite of piezoelectric ceramics, rare-earth iron alloys, and polymer. *Appl. Phys. Lett.* **81,** 3831–3833 (2002).
7. Srinivasan, G., Rasmussen, E. T., Levin, B. J. & Hayes, R. Magnetoelectric effects in bilayers and multilayers of magnetoresistive and piezoelectric perovskite oxides. *Phys. Rev. B* **65,** 134402 (2002).
8. Kimura, T. Magnetic control of ferroelectric polarization. *Nature* **426,** 55–58 (2003).
9. Van Aken, B. B., Palstra, T. T. M., Filippetti, A. & Spaldin, N. A. Origin of ferroelectricity in magnetoelectric $YMnO_3$. *Nature Mater.* **3,** 164–170 (2004).
10. Hur, N. *et al.* Electric polarization reversal and memory in multiferroic material induced by magnetic fields. *Nature* **429,** 392–395 (2004).
11. Coeuré, P., Guinet, F., Peuzin, J. C., Buisson, G. & Bertaut, E. F. in *Proc. Int. Meeting on Ferroelectricity* (ed. Dvorák, V.) 332–340 (Institute of Physics of the Czechoslovak Academy of Sciences, Prague, 1996).
12. Fiebig, M. *et al.* Determination of the magnetic symmetry of hexagonal manganites by second harmonic generation. *Phys. Rev. Lett.* **84,** 5620–5623 (2000).
13. Sugie, H., Iwata, N. & Kohn, K. Magnetic ordering of rare earth ions and magnetic-electric interaction of hexagonal $RMnO_3$ (R = Ho, Er, Yb or Lu). *J. Phys. Soc. Jpn* **71,** 1558–1564 (2002).
14. van Aken, B. B. *Structural Response to Electronic Transitions in Hexagonal and Ortho-Manganites.* Thesis, Reiksuniv. Groningen (2001).
15. Fiebig, M., Lottermoser, Th. & Pisarev, R. V. Spin-rotation phenomena and magnetic phase diagrams of hexagonal $RMnO_3$. *J. Appl. Phys.* **93,** 8194–8197 (2003).
16. Leute, S., Lottermoser, Th. & Fröhlich, D. Nonlinear spatially resolved phase spectroscopy. *Opt. Lett.* **24,** 1520–1522 (1999).
17. Maichle, J. K., Ihringer, J. & Prandl, W. Simultaneous structure refinement of neutron, synchrotron and x-ray powder diffraction patterns. *J. Appl. Crystallogr.* **21,** 22–28 (1998).
18. Ihringer, J. A quantitative measure for the goodness of fit in profile refinements with more than 20 degrees of freedom. *J. Appl. Crystallogr.* **28,** 618–619 (1995).
19. Rebmann, C., Ritter, H. & Ihringer, J. Standard uncertainty of angular positions and statistical quality of step-scan intensity data. *Acta Crystallogr. A* **54,** 225–231 (1998).
20. Fiebig, M., Fröhlich, D., Lottermoser, Th. & Maat, M. Probing of ferroelectric surface and bulk domains in ferroelectric $RMnO_3$ (R = Y, Ho) by second harmonic generation. *Phys. Rev. B* **66,** 144102 (2002).
21. Fox, D. L., Tilley, D. R., Scott, J. F. & Guggenheim, H. J. Magnetoelectric phenomena in $BaMnF_4$ and $BaMn_{0.99}Co_{0.01}F_4$. *Phys. Rev. B* **21,** 2926–2936 (1980).
22. Scott, J. F. Phase transitions in $BaMnF_4$. *Rep. Prog. Phys.* **42,** 1055–1084 (1979).
23. Ascher, E., Riedel, H., Schmid, H. & Stössel, H. Some properties of ferromagnetic nickel-iodine boracite $Ni_3B_7O_{13}I$. *J. Appl. Phys.* **37,** 1404–1405 (1966).
24. Fiebig, M., Degenhardt, C. & Pisarev, R. V. Interaction of frustrated magnetic sublattices in $ErMnO_3$. *Phys. Rev. Lett.* **88,** 027203 (2002).
25. Kritayakirana, K., Berger, P. & Jones, R. V. Optical spectra of ferroelectric-antiferromagnetic rare earth manganates. *Opt. Commun.* **1,** 95–98 (1969).
26. Dzyaloshinskii, I. E. Thermodynamic theory of 'weak' ferromagnetism in antiferromagnetic substances. *Sov. Phys. JETP* **5,** 1259–1272 (1957).
27. Fiebig, M., Eremenko, V. & Chupis, I. (eds) *Magnetoelectric Interaction Phenomena in Crystals* (Kluwer, Dordrecht, 2004).
28. Zheng, H. *et al.* Multiferroic $BaTiO_3$-$CoFe_2O_4$ nanostructures. *Science* **303,** 661–663 (2004).
29. Saxena, S. S. *et al.* Superconductivity on the border of itinerant-electron ferromagnetism in UGe_2. *Nature* **406,** 587–591 (2000).

Acknowledgements We thank K. Kohn and K. Hagdorn for samples, and the DFG and the BMBF for financial support. M. F. thanks T. Elsässer for continuous support.

Competing interests statement The authors declare that they have no competing financial interests.

Correspondence and requests for materials should be addressed to M.F. (fiebig@mbi-berlin.de).

Demixing in simple fluids induced by electric field gradients

Yoav Tsori, François Tournilhac & Ludwik Leibler

Laboratoire Matière Molle & Chimie (UMR 167 CNRS-ESPCI), Ecole Supérieure de Physique et Chimie Industrielles, 10 rue Vauquelin, 75231 Paris CEDEX 05, France

Phase separation in liquid mixtures is mainly controlled by temperature and pressure, but can also be influenced by gravitational, magnetic or electric fields. However, the weak coupling between such fields and concentration fluctuations limits this effect to extreme conditions[1–3]. For example, mixing induced by uniform electric fields is detectable only at temperatures that are within a few hundredths of degree or less of the phase transition temperature of the system being studied[4–7]. Here we predict and demonstrate that electric fields can control the phase separation behaviour of mixtures of simple liquids under more practical conditions, provided that the fields are non-uniform. By applying a voltage of 100 V across unevenly spaced electrodes about 50 μm apart, we can reversibly induce the demixing of paraffin and silicone oil at 1 K above the phase transition temperature of the mixture; when the field gradients are turned off, the mixture becomes homogeneous again. This direct control over phase separation behaviour depends on field intensity, with the electrode geometry determining the length-scale of the effect. We expect that this phenomenon will find a number of nanotechnological applications, particularly as it benefits from field gradients near small conducting objects.

The driving force for separation in liquid mixtures is the preference of constituent molecules to be in contact with their own species[8]. At high temperatures, however, thermal agitation dominates over enthalpic interactions, and mixing occurs. Figure 1a shows the classic phase diagram of a binary mixture of two liquids, A and B, with phase transition temperature, T_t (blue curve), as a function of the concentration of A (ϕ; where $0 < \phi < 1$). Above T_t

at point 'α', the two liquids are miscible (Fig. 1b); a quench to below T_t, to a point 'β', leads to creation of (say) A-rich droplets in a B-rich continuous phase. The appearance of an interface between demixed phases is a signature of the phase separation transition (Fig. 1c).

The effect of uniform electric fields on liquid phase separation has attracted considerable attention in the past 50 years[1,4–7,9,10]. And yet, even the question of whether the field favours mixing or demixing is still a subject of debate[5,9,11]. Indeed, the shift of the transition temperature caused by uniform fields can originate from the non-linear dependence of dielectric constant on composition[1,4] or from thermal composition fluctuations which in turn induce local electric field fluctuations[10,11]. Theories predict field induced phase separation[1,4,6,11] whereas most experiments show that uniform electric fields favour mixing[4–7]. Still, even for mixtures with a large dielectric constant mismatch, the effect is weak: the critical temperature decreases by about 0.015 K when a field of about 4 MV m^{-1} is applied[4,7]. However, and this is our starting point, the situation is very different when the applied field is non-uniform at a macroscopic scale. For weak fields, the mixture exhibits smooth concentration gradients, as shown schematically in Fig. 1d. This is a molecular analogue of the 'dielectric rise' effect, in which a dielectric liquid is pulled towards a region of high electric field by a dielectrophoretic force[1,12,13]. We show that when the electric field exceeds a critical value, the composition profile changes dramatically: the mixture phase separates, creating a sharp interface (Fig. 1e). Here, demixing originates from the direct coupling between composition and field, and, therefore, the effects are strong. For simple non-polar liquids, demixing can be induced as far as a few degrees above the transition temperature and with easily accessible fields. The new displaced phase lines are shown in green and red curves in Fig. 1a, for two different field amplitudes. The electric field induced demixing may be useful for various optical and chemical applications—and once phase separation is produced, external fields can drive electrohydrodynamic[14] and interfacial instabilities[15,16] or electro-wetting phenomena[17–19]. Upon switching off the electric field, a homogeneous mixture is recovered.

When an electric field is applied to a homogeneous non-conducting mixture, the electrostatic contribution of the free energy is given by F_{es}:

$$F_{es} = -\frac{1}{2}\int \varepsilon(\mathbf{r})\mathbf{E}^2(\mathbf{r})\mathrm{d}^3 r \qquad (1)$$

where ε denotes the dielectric constant, and $\mathbf{E}(\mathbf{r})$ is the local field at point $\mathbf{r}$ obeying the appropriate boundary conditions on the electrodes[1]. In a mixture of liquids A and B with dielectric constants ε_A and ε_B, respectively, ε depends on the composition of the mixture, $\phi(\mathbf{r})$. Local composition variations yield a spatially varying dielectric constant, and the system tries to adjust the mixture concentration and the local field in order to minimize the free energy.

Within a mean field approximation, the concentration profile $\phi(\mathbf{r})$ and local electric field E can be found by minimizing the free energy $F = \int f_b(\phi, T)\mathrm{d}^3 r + F_{es}$, with boundary conditions imposed by the electrode geometry. $f_b(\phi,T)$ is the free-energy density in the absence of electric field yielding the separation temperature $T_t(\phi)$ as shown in Fig. 1 (see Methods).

For arbitrary electrode geometry analytical solution is difficult. The 'wedge' geometry, consisting of two flat and planar tilted electrodes, is particularly simple and brings a useful insight (see Fig. 2a). Indeed, for any concentration profile $\phi(r)$ with azimuthal symmetry, the electric field $\mathbf{E}$ is perpendicular to $\nabla\varepsilon$ and in consequence the field $\mathbf{E}(\mathbf{r})$ is simply given by the solution of the Laplace equation $\nabla\cdot\mathbf{E} = 0$, namely, $E(r) = V/\theta r$, with V being the potential differences across the electrodes and θ the opening angle between them. This great simplification allows to find the composition profile $\phi(r)$ by solving the Euler–Lagrange equation $\delta f_b/\delta\phi - 1/2(\delta\varepsilon/\delta\phi)E^2(r) - \mu = 0$, with μ denoting the chemical potential. The analysis of this equation along classical lines[20] enables us to find the displacement ΔT of the transition temperature by the

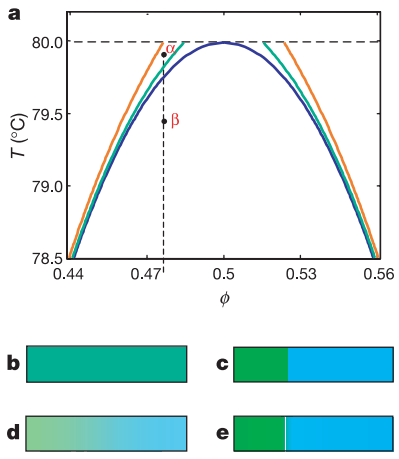

Figure 1 Phase diagram of a symmetric A/B liquid mixture. **a**, Transition temperature $T_t(\phi)$ in the absence of field (blue curve) and with a non-homogeneous field in the wedge geometry (ϕ is the fraction of A in the mixture). The green and red curves correspond to maximum fields of 8 and 15 V μm^{-1}, respectively. **b**, At point 'α' above T_t the mixture is homogeneous. **c**, At point 'β' below T_t the mixture phase separates. Green colour denotes B liquid, blue is A. **d**, Above T_t, a small field gradient induces a small concentration gradient. **e**, Above T_t, a large field gradient provokes phase separation. We used $\varepsilon_A - \varepsilon_B = 5$, $\partial^2\varepsilon/\partial\phi^2 = 5$, $v_0 = 3\times10^{-27}$ m^3 and scaled the critical temperature to be 80 °C.

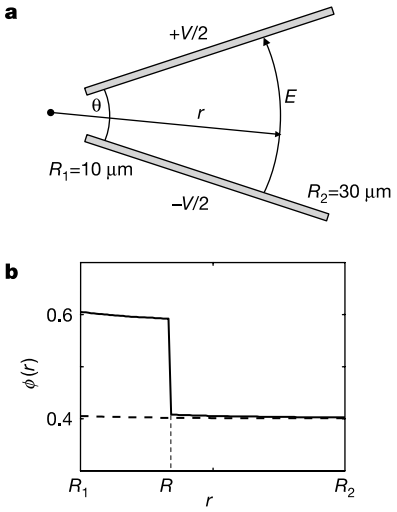

Figure 2 Wedge-shaped model system. **a**, The mixture is put between two flat electrodes with opening angle θ and potential difference V. Far from the edges, the field $E = V/\theta r$ is azimuthal. **b**, At points above the transition (for example, point 'α' of Fig. 1a) and for $\varepsilon_A > \varepsilon_B$, a small voltage V gives rise to a smoothly decaying profile $\phi(r)$, with high ϕ (large ε) at $r = R_1$ and low ϕ (small ε) at $r = R_2$, dashed curve. At the critical voltage V_c, the composition $\phi(R_1)$ becomes unstable. When $V > V_c$ a sharp transition is predicted between high- and low-ϕ regions, solid curve. $\phi(r)$ decays to the bulk average value at large r, here $\phi = 0.4$. We used a standard solution model for the bulk free energy f_b (see Methods section), $T = T_t + 0.2$ °C, $R_2 = 3R_1 = 30$ μm and other parameters as in Fig. 1.

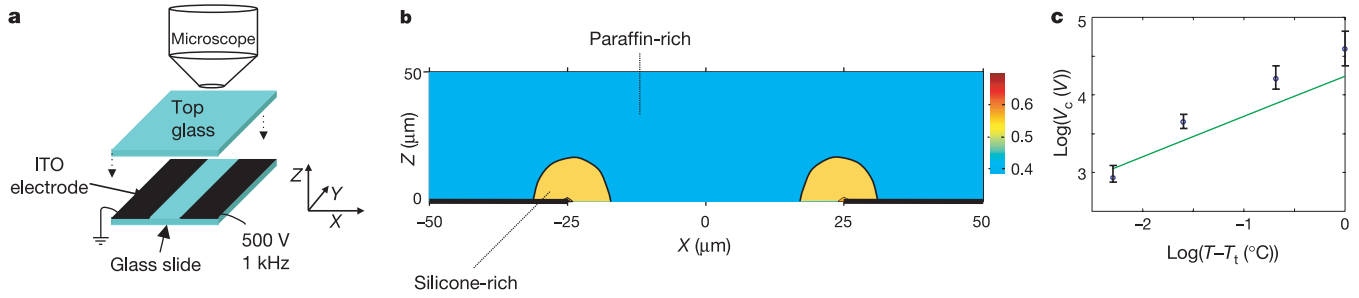

Figure 3 Phase separation with razor-blade electrodes. **a**, Two parts of the bottom glass substrate are coated with a conducting indium tin oxide layer, connected to opposite voltage terminals. The silicone/paraffin mixture between the substrate and the top glass is observed using an optical phase-contrast microscope. **b**, Predicted composition profile $\phi(r)$ in the $x - z$ plane numerically obtained for $V = 150$ V above the threshold. Black lines indicate the two flat electrodes. The silicone-rich phase appears close to the electrode edge, while the paraffin-rich phase is farther away. Here $\phi = 0.45$, $v_0 = 3 \times 10^{-27}\,\mathrm{m}^{-3}$ and $T - T_t = 0.2\,^{\circ}\mathrm{C}$. **c**, Plot of $V_c(T)$ for $T > T_t$. Straight green line (slope 0.5) is model calculation, while points are experimental values with best fit slope 0.7 ± 0.15. Error bars correspond to uncertainty in extrapolation in Fig. 4d.

above non-homogeneous field:

$$\Delta T \approx \frac{v_0}{k_B}\frac{1}{8\pi}\left|\frac{\varepsilon'}{\phi - \phi_c}\right|\left(\frac{V}{\theta R_1}\right)^2 \qquad (2)$$

Here k_B is the Boltzmann constant, v_0 the liquid molecular volume, ϕ_c the critical composition and $\varepsilon' \approx \varepsilon_A - \varepsilon_B$ the derivative of the dielectric constant $\varepsilon(\phi)$ with respect to composition taken at ϕ_c. In equation (2), $r = R_1$ is the position of the inner edge of the wedge (Fig. 2a) where the field is strongest. The transition temperature is thus shifted upwards in the phase diagram (field provokes demixing) and ΔT is proportional to ε' (Fig. 1a). The estimate, equation (2), is valid for compositions ϕ such that $T_t(\phi) + \Delta T \leq T_c$. At compositions ϕ closer to ϕ_c, phase separation occurs at the critical temperature T_c (or just slightly above it when the nonlinear dependence of ε on ϕ plays some role).

The change in T_t by non-uniform fields is large even for mixtures with a weak dielectric constant mismatch, $\varepsilon_A - \varepsilon_B \approx 1$. An estimate with voltage $V = 100$ V, small feature size $R_1 = 10\,\mu$m, $\theta = 1$ and $\phi = 0.4$ ($|\phi - \phi_c| \approx 0.1$) yields an upward shift of about $\Delta T \approx 0.2\,^{\circ}$C. Larger dielectric contrast ε' or smaller distance from the critical composition results in correspondingly larger ΔT.

The phase separation by a non-uniform field is much stronger than the effect of a uniform field. In a uniform field E_0, it can be shown within the same approximations that ΔT is given by $\Delta T \approx \frac{1}{16\pi}(v_0/k_B)\varepsilon'' E_0^2$ (ref. 1). This shift is proportional to the second derivative of dielectric constant with respect to the composition ε'' and relies on second-order coupling of electric field and composition variations. Typically $\varepsilon'' \approx \varepsilon'$, and the shift ΔT in uniform field is about 10 to 50 times smaller than that in non-uniform fields, equation (2). We recall, however, that experimentally for liquid mixtures uniform field causes mixing rather than phase separation.

A useful insight into field-induced separation is gained by analysing the evolution of the composition profile for the wedge electrode geometry. When $\varepsilon' = \varepsilon_A - \varepsilon_B > 0$ and for low voltage V, the composition $\phi(R_1)$ at the inner edge is higher than $\phi(R_2)$ at the outer edge, and the profile $\phi(r)$ is a smoothly decaying function of r (Fig. 2b, dashed curve). However, at a given temperature $T \leq T_c$, there exists a threshold voltage V_c where the behaviour changes markedly. Referring to Fig. 1, the composition $\phi(R_1)$ becomes unstable when it crosses the transition curve $T_t(\phi)$, and separation occurs. An interface between A-rich (high ε) and B-rich (low ε) regions appears at $r = R$ (Fig. 2b, solid curve). The concentration profile then exhibits a sharp jump even though the field, $E(r) = V/\theta r$, still varies smoothly. When the voltage difference V increases, the interface moves towards the outer edge. From equation (2), the critical voltage V_c necessary to produce phase separation scales as $V_c \approx (T - T_t)^{1/2}$.

To test the above predictions, we used the experimental set-up shown in Fig. 3a. We chose to work with razor-shaped electrodes with sharp edges in order to take advantage of the large field gradients present in such a geometry. Figure 3b shows typical concentration profiles calculated by numerical minimization of the total free energy for voltage above the threshold. Two interfaces parallel to each electrode should appear in the region close to the electrode edge. Raising the field (voltage) should displace the interfaces farther from the electrode edge, and should also increase the composition difference between coexisting phases. Lowering the temperature towards T_t while keeping the voltage fixed has a similar effect. As shown in Fig. 3c the threshold voltage V_c and the field at the electrode tips are expected to be low (below the dielectric breakdown) even for temperatures well above T_t.

We worked with two liquid pairs: a mixture of an aromatic silicone oil (polymethylphenylsiloxane) and a low-molecular-mass

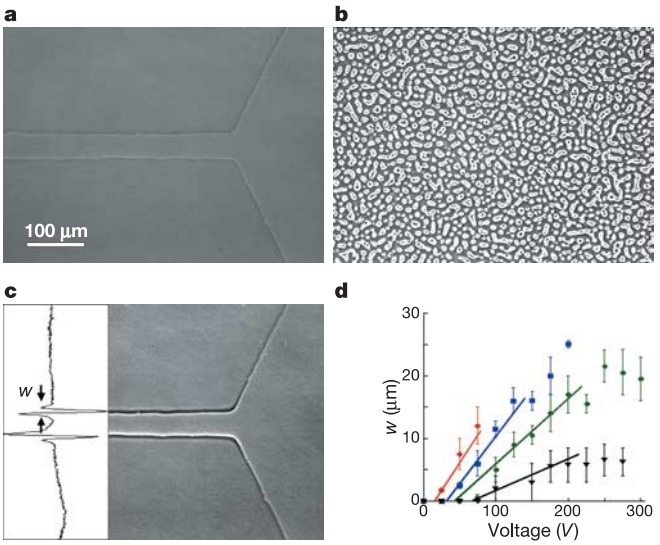

Figure 4 Temperature and voltage dependence of phase separation. **a**, The mixture is in the homogeneous state at $T = T_t + 0.1\,^{\circ}$C, and no voltage is applied. **b**, At $T = T_t - 0.3\,^{\circ}$C, isotropic phase separation occurs, in which drops begin to grow until macro-phase separation. **c**, At $T = T_t + 0.2\,^{\circ}$C and $V = 200$ V, a silicone-rich channel appears along the electrode edges. **d**, Width w of silicone-rich phase close to the edge of the electrodes, plotted as a function of applied voltage V, for temperatures 0.1 (diamonds), 0.3 (squares), 0.5 (circles) and 1 (triangles) °C above T_t. Symbols are experimental data, while solid lines are results of numerical calculation (see Methods section). Error bars correspond to the scatter of three different measurements.

paraffin oil (squalane), and a mixture of low-molecular-mass polydimethylsiloxane and polyisobutylene. We chose these systems because they are non-volatile, non-polar and have a good electric breakdown resistance. We were able to observe electric field induced demixing in both systems despite their modest dielectric constant mismatch.

Below T_t, phase separation is visible across the whole specimen (Fig. 4b). There is no preferential nucleation or wetting at the electrodes. Experiments with the electric field were performed at temperatures above T_t, namely $T - T_t = 0.1$, 0.3, 0.5 and 1 °C. The influence of heating due to dielectric losses and conduction of residual ions was verified to be negligible at the working frequencies. Moreover, heating increases the temperature and opposes demixing.

Phase separation occurs immediately after the electric field is switched on, and interfaces parallel to the electrodes appear (Fig. 4c). Demixing patterns typically evolve over 1 minute, after which a channel of the silicone-rich phase (more polar liquid) is formed along the electrodes' boundaries. This nicely agrees with the numerical calculation for this electrode geometry. When the voltage is switched off, the mixture returns back to its homogeneous state in 4–5 min (Fig. 4a). The phase separation process is reversible and can be repeated many times. The universal character of field induced separation is confirmed by investigations of mixtures of polydimethylsiloxane and polyisobutylene and using different electrode spacing.

The width w of the silicone domain close to the electrode edge increases when the applied voltage is increased or when temperature is reduced closer to T_t. Figure 4d shows a plot of w as a function of V at four temperatures. There is a good agreement between the experimental points and the values obtained by numerically minimizing the free-energy functional. The theoretical and experimental critical voltages V_c, obtained from the extrapolation of each curve to the $w = 0$ axis, also agree reasonably well (Fig. 3c).

The phase separation by non-uniform electric fields is robust and, as indicated by equation (2), can be used on many liquid mixtures well below dielectric breakdown. This complements nicely the gradient field induced phase transitions in colloidal suspensions[21,22] and ferrofluids[23]. Various microfluidic or micro-electromechanical devices could benefit from this effect. For example, a mixture of several components flowing down a channel could be separated and sent off in different channels. Such a separation could provide a new way to reversibly coat the walls of the channel with a preferred chemical species and efficiently control lubrication. Chemically reactive systems could benefit as well, because active species could be isolated from each other or brought together by the electric field, thus achieving better control of reaction kinetics. Phase separation could be also employed to create reversible electro-optic effects in light guiding, scattering, and so on. In this work, non-uniform fields were created by conducting electrodes. Use of holographic optical tweezers techniques[24,25] may open a new field of applications, such as patterning and writing. In all these applications, the reversibility of the process and the dependence on field intensity is a boon. □

Methods

Experimental

Polymethylphenylsiloxane (CAS number: 9005-12-3, Gelest PMM-0025), with a mass average molecular weight of 3,000 g mol^{-1} and a polydispersity index of 2.4, and squalane (CAS number: 111-01-3, purity: 99.8%) were used without further purification. Transparent indium tin oxide (ITO) electrodes 25 nm thick (surface resistivity: 120 Ω per square) were coated on the substrate glass using Shipley SJR 5740 photoresist and HCl/HNO_3 as etchant. Observation cells were made up of the ITO-treated substrate covered with a top glass layer. The temperature was regulated using a Mettler FP80 hot stage, and checked to be stable within ±0.03 °C using a Pt100 probe. Before experiments, the thickness of the empty cell was measured by varying the focus of the microscope. The mixtures were heated about 20 °C above their cloud point temperature before being put in the cell. The cloud point of each specimen was carefully measured through cooling cycles of −1 °C min^{-1} and −0.1 °C min^{-1}.

The high-voltage 1 kHz a.c. source was built from a Sefram 4430 signal generator fitted with an 18 W audio amplifier and a standard 12 V car-engine coil. Optical observations were carried out in phase contrast mode using a Leica DMRD microscope equipped with a filtered (transmission maximum at 544 nm) incandescent source and Fluotar 10 × 0.30 objective. Images were digitized using a JVC 3CCD camera and Eurocard Picolo video board. The width w of the silicone-rich phase near the electrodes was measured from the series of light intensity fringes in the phase contrast image, as defined in the inset of Fig. 4c.

Theoretical

The numerical calculation used in Fig. 2b, Fig. 3b and c, and Fig. 4d is obtained from a variational principle of the total free energy $F = F_b + F_{es}$ with respect to the local concentration ϕ and field E:

$$\frac{\delta f_b(\phi)}{\delta \phi} - \frac{1}{2}\frac{\delta \varepsilon}{\delta \phi}\mathbf{E}^2 - \mu = 0 \quad (3a)$$

$$\nabla\cdot(\varepsilon\mathbf{E}) = 0 \quad (3b)$$

where μ is the chemical potential. The bulk free-energy density f_b is given by a Landau expansion of a standard mean-field symmetric solution model around the critical point[20,26], $\frac{v_0}{k_B T} f_b = \frac{1}{2}\frac{T-T_c}{T_c}\left(\phi - \frac{1}{2}\right)^2 + \frac{4}{3}\left(\phi - \frac{1}{2}\right)^4$, where k_B is the Botlzmann constant, v_0 is the molecular volume, T_c is the critical temperature and $\phi = 1/2$ is the critical composition. Solutions to equations (3a) and (3b) were obtained by a combination of a standard matrix inversion method for the Laplace equation and an iterative gradient scheme for the concentration profile equation.

Received 27 November 2003; accepted 14 June 2004; doi:10.1038/nature02758.

1. Landau, L. D. & Lifshitz, E. M. *Elektrodinamika Sploshnykh Sred* Ch. II, Sect. 18, problem 1 (Nauka, Moscow, 1957).
2. Greer, S. C., Block, T. E. & Knobler, C. M. Concentration gradients in nitroethane+3-methylpentane near the liquid-liquid critical solution point. *Phys. Rev. Lett.* **34,** 250–253 (1975).
3. Moldover, M. R., Sengers, J. V., Gammon, R. V. & Hocken, R. J. Gravity effects in fluids near gas-liquid critical point. *Rev. Mod. Phys.* **51,** 79–99 (1979).
4. Debye, P. & Kleboth, K. Electrical field effect on the critical opalescence. *J. Chem. Phys.* **42,** 3155–3162 (1965).
5. Early, M. D. Dielectric constant measurements near the critical point of cyclohexane-aniline. *J. Chem. Phys.* **96,** 641–647 (1992).
6. Wirtz, D. & Fuller, G. G. Phase transitions induced by electric fields in near-critical polymer solutions. *Phys. Rev. Lett.* **71,** 2236–2239 (1993).
7. Orzechowski, K. Electric field effect on the upper critical solution temperature. *Chem. Phys.* **240,** 275–281 (1999).
8. Rowlinson, J. S. & Swinton, F. S. *Liquids and Liquid Mixtures* (Butterworths, London, 1982).
9. Sengers, J. V., Bedeaux, D., Mazur, P. & Greer, S. C. Behavior of the dielectric constant of fluids near a critical point. *Physica. A* **104,** 573–594 (1980).
10. Amundson, K., Helfand, E., Quan, X. N., Hudson, S. D. & Smith, S. D. Alignment of lamellar block-copolymer microstructure in an electric-field. 2. Mechanisms of alignment. *Macromolecules* **27,** 6559–6570 (1994).
11. Onuki, A. Electric-field effects in fluids near the critical point. *Europhys. Lett.* **29,** 611–616 (1995).
12. Pohl, H. A. *Dielectrophoresis* (Cambridge Univ. Press, Cambridge, UK, 1978).
13. Christen, T. Homogenization of nonuniform electric fields in mixtures of liquid dielectrics. *Appl. Phys. Lett.* **76,** 230–232 (2000).
14. Melcher, J. R. & Taylor, G. I. Electrohydrodynamics—A review of the role of interfacial shear stresses. *Annu. Rev. Fluid Mech.* **1,** 111–146 (1969).
15. Schäffer, E., Thurn-Albrecht, T., Russell, T. P. & Steiner, U. Electrically induced structure formation and pattern transfer. *Nature* **403,** 874–877 (2000).
16. Tsori, Y. & Andelman, D. Thin film diblock copolymers in electric field: Transition from perpendicular to parallel lamellae. *Macromolecules* **35,** 5161–5170 (2002).
17. Berge, B. & Peseux, J. Variable focal lens controlled by an external voltage: An application of electrowetting. *Eur. Phys. J. E* **3,** 159–163 (2000).
18. Comiskey, B., Albert, J. D., Yoshizawa, H. & Jacobson, J. An electrophoretic ink for all-printed reflective electronic displays. *Nature* **394,** 253–255 (1998).
19. Pollack, M. G., Fair, R. B. & Shenderov, A. D. Electrowetting-based actuation of liquid droplets for microfluidic applications. *Appl. Phys. Lett.* **77,** 1725–1726 (2000).
20. Lifshitz, E. M. & Landau, L. D. *Statistical Physics* 2nd edn (Butterworth-Heinemann, New York, 1980).
21. Khusid, B. & Acrivos, A. Effects of interparticle electric interactions on dielectrophoresis in colloidal suspensions. *Phys. Rev. E* **54,** 5428–5435 (1996).
22. Kumar, A., Qiu, Z., Acrivos, A., Khusid, B. & Jacqmin, D. Combined negative dielectrophoresis and phase separation in nondilute suspensions subject to a high-gradient ac electric field. *Phys. Rev. E* **69,** 021402 (2004).
23. Rosensweig, R. E. *Ferrohydrodynamics* (Dover, New York, 1998).
24. Korda, P. T., Taylor, M. B. & Grier, D. G. Kinetically locked-in colloidal transport in an array of optical tweezers. *Phys. Rev. Lett.* **89,** 128301 (2002).
25. Grier, D. G. A revolution in optical manipulation. *Nature* **424,** 810–816 (2003).
26. De Gennes, P. G. *Scaling Concepts in Polymer Physics* (Cornell Univ. Press, Ithaca, New York, 1979).

Supplementary Information accompanies the paper on **www.nature.com/nature**

Acknowledgements We thank D. Andelman and P. G. de Gennes for discussions and suggestions, and R. Bonnecaze and A.-V. Ruzette for comments on the manuscript. We gratefully acknowledge support from ATOFINA.

Competing interests statement The authors declare that they have no competing financial interests.

Correspondence and requests for materials should be addressed to L.L. (Ludwik.leibler@espci.fr).